



## Biodegradability enhancement of azo dye Direct Orange-26 using UV/Fenton-like process: optimization using response surface methodology

Zahra Parsa<sup>a</sup>, Mohsen Motevassel<sup>a</sup>, Mohammad Reza Khosravi-Nikou<sup>a,b,\*</sup>, Sahand Jorfi<sup>c,d</sup>, Bahram Ghasemi<sup>a</sup>

<sup>a</sup>Department of Chemical Engineering, Petroleum University of Technology, Abadan, Iran,

emails: zari.parsa.2011@gmail.com (Z. Parsa), motavassel@put.ac.ir (M. Motevassel), b.ghasemi@put.ac.ir (B. Ghasemi)

<sup>b</sup>Department of Gas Engineering, Petroleum University of Technology, Ahwaz, Iran, email: mr.khosravi@put.ac.ir

<sup>c</sup>Environmental Technologies Research Center, Ahwaz Jundishapur University of Medical Sciences, Ahwaz, Iran

<sup>d</sup>Department of Environmental Health Engineering, School of Health, Ahwaz Jundishapur University of Medical Sciences, Ahwaz, Iran, email: sahand369@yahoo.com

Received 10 January 2017; Accepted 27 June 2017

### ABSTRACT

In the present study, the enhancement of biodegradability of Direct Orange-26 (azo dye) in aqueous solution by photo-Fenton-like process and nano-Fe<sub>2</sub>O<sub>3</sub> as catalyst was investigated. The effects of initial pH, reaction time, initial concentration of nano-Fe<sub>2</sub>O<sub>3</sub>, and H<sub>2</sub>O<sub>2</sub> dosage on the biochemical oxygen demand (BOD<sub>5</sub>)/chemical oxygen demand (COD) ratio were studied in batch process using response surface methodology. The analysis of variance suggested that the optimal conditions for enhancement of biodegradability of azo dye solution to be counted as a biodegradable effluent are as follows: nano-Fe<sub>2</sub>O<sub>3</sub> concentration of 0.23 g L<sup>-1</sup>, H<sub>2</sub>O<sub>2</sub> concentration of 64 mM, pH of 7.5, and the reaction time of 21.66 min. The BOD<sub>5</sub>/COD ratio at optimal condition was predicted to be 0.50 and confirmed by the experimental study. A good agreement between the model prediction and experimental results confirms the reliability of the developed model for BOD<sub>5</sub>/COD ratio.

*Keywords:* UVC; Fenton-like; Direct Orange-26; Nano-Fe<sub>2</sub>O<sub>3</sub>; BOD<sub>5</sub>/COD ratio

### 1. Introduction

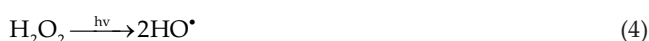
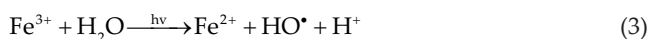
Recalcitrant wastewater includes materials that are resistant to biological degradation. These wastewaters are characterized by high chemical oxygen demand (COD) and low biochemical oxygen demand (BOD) [1]. Recalcitrant organic compounds originate from various industries such as chemicals, petrochemicals, textile, refinery and cellulosic and are released to the environment [2]. Recalcitrant contained wastewaters are toxic to the health and environment [3,4] and would be strictly treated through application complicated and expensive physical and chemical methods. Researchers have argued that chemical treatment methods like advanced oxidation

processes (AOPs) can be considered as a pre-treatment step to enhance the biodegradability of wastewater (according to BOD<sub>5</sub>/COD ratio) and subsequently a biological treatment process to obtain targets would be a cost-effective and efficient scheme to minimize side effects of chemical processes as a single process for the complete treatment of industrial wastewater. BOD<sub>5</sub>/COD ratio is an acceptable index to observe the variations of wastewater biodegradability [5,6]. Generally, a wastewater sample with BOD<sub>5</sub>/COD ratio of 0.4–0.5 would be considered biodegradable and conversely, the fewer amounts is resistant to biological treatment [5]. Azo dyes with one or more nitrogen double bonds (–N=N–) consist of the largest class of dyes [7–9]. Contamination of the environment by azo dyes results in harmful effects on humans and animals such as carcinogenic and mutagenic effects [8]. Therefore, the treatment of azo dye-contained wastewaters is

\* Corresponding author.

an important issue in the event of the environment and public health. Azo dyes are used in textile, leather and plastic industries [10]. Azo dye-containing effluents are among the most resistant wastewaters due to their low biodegradability and high COD and huge such flow would be produced annually by afore-mentioned industries [11]. According to Bahmani et al. [8], more than  $7 \times 10^5$  tons of synthetic dyes are produced annually by textile industries, of which  $2.8 \times 10^5$  tones are discharged. Recent studies showed that so-called advanced oxidation processes are a good option to degrade recalcitrant compounds and treatment of such wastewaters [11–14]. The application of these processes is based on the generation of active and non-selective hydroxyl radicals that attack the organic matter in wastewater [15–17]. The end products of a complete oxidation of recalcitrant materials by AOPs would be  $\text{CO}_2$ ,  $\text{H}_2\text{O}$  and mineral salts that are non-toxic outputs [14,18,19]. Among different AOPs, Fenton-based oxidation is proved to be an efficient and attractive process, in which,  $\text{HO}^\bullet$  radicals are generated through reaction between iron ions and hydrogen peroxide ( $\text{H}_2\text{O}_2$ ) [20]. Fenton process uses conventional equipment and operates at ambient pressures and temperatures. However, this process has some drawbacks due mainly to the formation of different Fe(III) complexes as solution pH changes. The optimum pH for the homogeneous Fenton process is about 2.8 when the iron in solution occurs partly as Fe(III) and partly as  $\text{Fe(III)(OH)}^{2+}$ , representing the photo-active species. Below this pH, the hydroxyl radicals are scavenged by protons and the concentration of  $\text{Fe(III)(OH)}^{2+}$  decreases while above this pH, Fe(III) precipitates as an oxyhydroxide. In order to maintain a pH of 3, large amounts of acid must be added to the reaction medium. Thus, it is impractical to apply the homogeneous Fenton process to in situ environmental remediations because large amount of ferric hydroxide sludge would be produced, creating disposal and other environmental problems [21–27]. To overcome these disadvantages, the photo-Fenton-like process is a good choice due to its capability at neutral pH or nearly neutral pH with less generation of iron-containing sludge.

In the photo-Fenton-like process,  $\text{HO}^\bullet$  radicals are generated through the reaction between  $\text{Fe}^{3+}$  ions and  $\text{H}_2\text{O}_2$  as well as the UV irradiation, which increased  $\text{HO}^\bullet$  generation [Eqs. (1)–(4)][28]:



The advantage of nano-iron catalyst in this reaction is due to providing complete oxidation of catalyst. For iron catalyst in the size of larger than nano, during the oxidation, a layer of iron oxide is formed on the particles and prevents the oxidation of inner side of catalyst [29]. In addition, high surface area leads to increasing in contact between catalyst and  $\text{H}_2\text{O}_2$ , and this property is nearby to homogeneous catalyst performance. On the other hand, separation and recovery of

heterogeneous nano-catalyst from solution is so easy due to insolubility of catalyst [1]. In addition, a combination of UV process with the Fenton-like process could increase the efficiency of the process and reduce the remaining time in the reactor, subsequently, could increase the efficiency of AOP.

Application of AOPs to complete mineralization of recalcitrant wastewater is a very expensive method. To reduce the costs of processes, AOPs can be used as a pre-treatment stage. So the biodegradability of recalcitrant wastewater enhanced with AOPs, until it is considered as a biodegradable wastewater.

Using conventional optimization method for different factors such as initial pH,  $\text{H}_2\text{O}_2$  concentration, reaction time and nano- $\text{Fe}_2\text{O}_3$  concentration in this process is not suitable [7,8,14,15,28,30]. The majority of recent studies concerned with the effects of these process parameters on the photo-Fenton-like process efficiency were performed using a one-factor-at-a-time approach, where this approach assesses one parameter at a time instead of all simultaneously. The method is time-consuming, expensive and often leads to misinterpretation of results when interactions between different components are present. To overcome these drawbacks, one of the statistical design tools, so-called response surface methodology (RSM), can be used for process optimization and prediction of interaction between several process parameters and one or more dependent parameters [31–33]. RSM is a reliable and powerful statistical method to design multifactor systems and optimization by considering the interaction between parameters [7,28,34].

In the current study, the performance of photo-Fenton-like oxidation process on the enhancement of biodegradability of azo dye (Direct Orange-26) was investigated. The influence of operational parameters such as initial pH,  $\text{H}_2\text{O}_2$  concentration, reaction time and nano- $\text{Fe}_2\text{O}_3$  concentration were evaluated and optimization performed by RSM.

## 2. Materials and methods

### 2.1. Materials

In order to prepare recalcitrant wastewater of textile industry, Direct Orange-26 with the structure shown in Fig. 1 was used in aqueous solution. The solution was prepared by dissolving 1.0 g of dye in 1,000 mL of distilled water. At this concentration of dye ( $1 \text{ g L}^{-1}$ ), the values of COD and BOD are  $1,890 \text{ mg L}^{-1}$  and  $570 \text{ mg L}^{-1}$ , respectively. The resulted  $\text{BOD}_5/\text{COD}$  ratio is 0.3, which is considered as recalcitrant wastewater. Iron oxide nano-powder (nano- $\text{Fe}_2\text{O}_3$ ) was purchased from US Research Nanomaterials, Inc. and used as received without further purification. Sodium hydroxide (>96%, Merck) and sulfuric acid (95%–97% Merck) were used to adjust pH. Hydrogen peroxide (30%, w/w) and methanol (99.9%) were purchased from Merck and used as received without any purification.

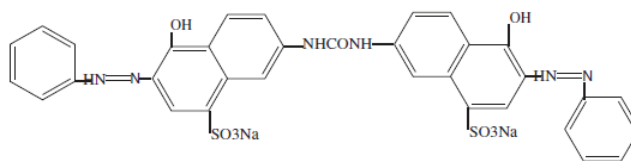


Fig. 1. Chemical structure of Direct Orange-26 [10].

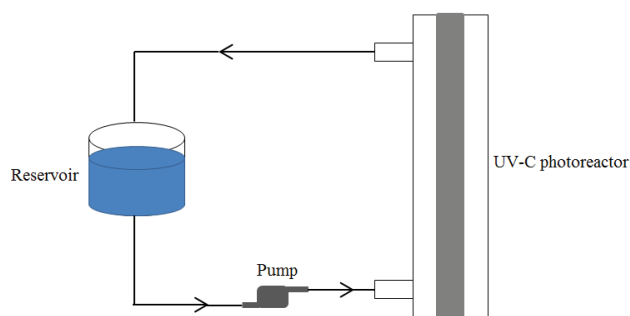


Fig. 2. Schematic view of the reactor.

## 2.2. Experimental setup

The degradation of azo dye from synthetic wastewater performed in a batch reactor. Applied schematic diagram of photoreactor in this study is shown in Fig. 2. Rectangular cubic glass photoreactor with the volume of 480 mL (4 cm × 4 cm × 30 cm) was used. The UV sources installed above the reactor included two 8-W UV-C lamps in all cases. The reactor contents were mixed with an agitator and 200 mL of synthetic wastewater was introduced to the photoreactor in all experiments.

## 2.3. Experimental procedure

Experiments were performed at room temperature (25°C ± 2°C). At first, initial pH was adjusted with addition of 0.1 M NaOH or 0.1 M H<sub>2</sub>SO<sub>4</sub>. Then nano-Fe<sub>2</sub>O<sub>3</sub> catalyst was added to the solution and a sample was taken under continuous stirring of the vessel to ensure sufficient aeration at the same time. Thereafter, the reaction solution was located under the UV-C lamp which was turned on 30 min before the start of the reaction to obtain a constant light emission. Advanced oxidation reaction was initiated by the addition of proper amounts of H<sub>2</sub>O<sub>2</sub> oxidant. To reduce scavenging effect, hydrogen peroxide was added continuously [11]. The sample was taken out at the end of experiments time and immediately mixed with 0.1 mL methanol to quench the reaction. At the end of experiments, COD and BOD concentration of samples were analyzed [34].

In order to optimize the independent variables (pH, reaction time, H<sub>2</sub>O<sub>2</sub> concentration and nano-Fe<sub>2</sub>O<sub>3</sub> concentration) in the photo-Fenton-like process, a central composite design (CCD) which is a popular form of RSM was applied [11,34,35]. The levels of independent variables were chosen according to preliminary experiments and literature (Table 1). Four-factor with three-level design produced 30 experimental runs. It included 16 factorial, 6 central and 8 axial points. The total number of experiments could be calculated from the following equation:

$$N = k^2 + 2k + C_p \quad (5)$$

where  $k$  is the factor number and ( $C_p$ ) is the replicate number of the central point [36].

Table 1  
Independent variables and the level used in experiments

Independent variables	Coded levels		
	-1	0	1
pH	3	6	9
Reaction time (min)	20	50	80
[H <sub>2</sub> O <sub>2</sub> ] (mM)	50	275	500
[nano-Fe <sub>2</sub> O <sub>3</sub> ] (g L <sup>-1</sup> )	0.15	1	1.85

At this study, BOD<sub>5</sub>/COD ratio was considered as the response of the photo-Fenton-like system. In CCD, the relation between response and independent variables was expressed by the following quadratic equation [11,28,34,35].

$$Y = b_0 + \sum_{i=1}^k b_i x_i + \sum_{i=1}^k b_{ii} x_i^2 + \sum_{i=1}^{k-1} \sum_{j=1}^k b_{ij} x_i x_j \quad (6)$$

where  $Y$  is the predicted response,  $x_i$  is an independent variable,  $b_0$  is the constant coefficient and  $b_i$ ,  $b_{ii}$  and  $b_{ij}$  are the interaction coefficients.

## 2.4. Analytical methods

The COD content of wastewater was measured according to ISO 6060, with closed reflux titrimetric method [7]. The BOD content was measured according to standard method 5210 B.

## 3. Results and discussion

### 3.1. Model results

Table 2 shows the observed and predicted results of BOD<sub>5</sub>/COD ratio for the different experimental conditions. For all the experiments, the initial BOD<sub>5</sub>/COD were 0.3. An empirical relation between BOD<sub>5</sub>/COD and independent variables suggested by the software is as follows:

$$\begin{aligned} \text{BOD}_5/\text{COD} = & -0.20515 + 0.26071 \times (\text{pH}) + 3.66453 \times 10^{-3} \times (\text{time}) \\ & + 1.1154010^{-3} \times [\text{H}_2\text{O}_2] + 0.19188 \times [\text{nano-Fe}_2\text{O}_3] \\ & - 3.333310^{-4} \times (\text{pH}) \times (\text{time}) - 7.4074110^{-5} \times (\text{pH}) \\ & \times [\text{H}_2\text{O}_2] - 9.8039210^{-4} \times (\text{pH}) \times [\text{nano-Fe}_2\text{O}_3] \\ & + 3.1481510^{-6} \times (\text{time}) \times [\text{H}_2\text{O}_2] - 3.4313710^{-4} \\ & \times (\text{time}) \times [\text{nano-Fe}_2\text{O}_3] - 1.9607810^{-5} \times [\text{H}_2\text{O}_2] \\ & \times [\text{nano-Fe}_2\text{O}_3] - 0.023928 \times (\text{pH})^2 - 5.9454210^{-6} \\ & \times (\text{time})^2 - 1.0933510^{-6} \times ([\text{H}_2\text{O}_2])^2 - 0.062769 \\ & \times ([\text{nano-Fe}_2\text{O}_3])^2 \quad (7) \end{aligned}$$

### 3.2. Statistical analysis

Table 3 shows analysis of variance (ANOVA) for the above suggested model to check the suitability, competence and fitness of model [3,35]. Generally,  $p$  value less than 0.05 shows the model is significant, while the value more than 0.1 is considered as insignificant. From the table, it is clear that the proposed model for BOD<sub>5</sub>/COD is significance (less than 0.0001). According to Table 3, pH, time, [H<sub>2</sub>O<sub>2</sub>], [nano-Fe<sub>2</sub>O<sub>3</sub>],

Table 2  
The results of enhancement of BOD<sub>5</sub>/COD ratio

Run	Independent coded variables				BOD <sub>5</sub> /COD	
	pH	Reaction time	[H <sub>2</sub> O <sub>2</sub> ]	[nano-Fe <sub>2</sub> O <sub>3</sub> ]	Observed	Predicted
1	-1	-1	-1	-1	0.51	0.48
2	1	-1	-1	-1	0.26	0.26
3	-1	1	-1	-1	0.6	0.61
4	1	1	-1	-1	0.3	0.27
5	-1	-1	1	-1	0.62	0.64
6	1	-1	1	-1	0.25	0.22
7	-1	1	1	-1	0.87	0.86
8	1	1	1	-1	0.29	0.32
9	-1	-1	-1	1	0.6	0.58
10	1	-1	-1	1	0.34	0.35
11	-1	1	-1	1	0.65	0.67
12	1	1	-1	1	0.34	0.32
13	-1	-1	1	1	0.7	0.72
14	1	-1	1	1	0.3	0.29
15	-1	1	1	1	0.9	0.9
16	1	1	1	1	0.33	0.35
17	-1	0	0	0	0.81	0.79
18	1	0	0	0	0.37	0.4
19	0	-1	0	0	0.72	0.76
20	0	1	0	0	0.88	0.85
21	0	0	-1	0	0.66	0.71
22	0	0	1	0	0.84	0.8
23	0	0	0	-1	0.7	0.73
24	0	0	0	1	0.82	0.8
25	0	0	0	0	0.8	0.81
26	0	0	0	0	0.85	0.81
27	0	0	0	0	0.78	0.81
28	0	0	0	0	0.86	0.81
29	0	0	0	0	0.83	0.81
30	0	0	0	0	0.79	0.81

(pH × time), (pH × [H<sub>2</sub>O<sub>2</sub>]), (time × [H<sub>2</sub>O<sub>2</sub>]), pH<sup>2</sup>, [H<sub>2</sub>O<sub>2</sub>]<sup>2</sup> are significant model terms. The *F* value of 1.42 for the lack of fit shows it is not significant to the pure error. It means that the model fit experimental data very well.

Figs. 3(a) and (b) show the normal plot of residuals and residuals vs. predicted values, respectively. It may be said that the residuals have a normal distribution when the points placed on a straight line, as shown in the figures [37,38]. It can be said that the suggested model is sufficiently acceptable to estimate the prediction of experimental data, while the points on the residual vs. predicted plot spread all over the area randomly (Fig. 3(b)) [28].

### 3.3. Effect of pH and time on BOD<sub>5</sub>/COD ratio

Figs. 4(a) and (b) show the counter and 3D response surface plot of pH and time in terms of BOD<sub>5</sub>/COD ratio, respectively. It is obvious that there is a maximum for BOD<sub>5</sub>/COD ratio when the pH varied from 3 to 9. In addition, BOD<sub>5</sub>/COD

ratio increased as reaction time increased. The maximum biodegradability reaches 0.91 when the pH is 4.5. The BOD<sub>5</sub> measurement methods are based on bacterial degradation, therefore, only the biodegradable part of wastewater could appear in the form of BOD<sub>5</sub> content. The behavior of pH may be explained by the fact that before the process, a large amount of pollutant organic matters appeared in the form of COD content due to its biodegradability resistance. After the process, recalcitrant matters convert to intermediate metabolites due to partial oxidation. These intermediate metabolites have a lower biodegradability resistance compared with the primary recalcitrant pollutant. Hence, intermediate metabolites appeared in the form of increasing BOD<sub>5</sub> content and partial oxidation of recalcitrant matters caused to decrease COD content. In the other words, COD content was decreased and BOD<sub>5</sub> content was increased, so BOD<sub>5</sub>/COD ratio was increased. For higher pH values, a reduction in BOD<sub>5</sub>/COD ratio was detected because of decrease in free iron species due to ferric oxyhydroxide precipitation, the formation of different complex species and breakdown of H<sub>2</sub>O<sub>2</sub> to O<sub>2</sub> and H<sub>2</sub>O. This fact resulted in the production of free radical HO• significantly, so a large amount of COD and BOD content remained unchanged and BOD<sub>5</sub>/COD ratio was decreased. While the reaction time increased the partial oxidation continued. Therefore, more COD content converted to intermediate metabolites and caused an increasing in BOD<sub>5</sub>/COD ratio.

### 3.4. Effect of pH and H<sub>2</sub>O<sub>2</sub> concentration on BOD<sub>5</sub>/COD ratio

The effect of pH and H<sub>2</sub>O<sub>2</sub> concentration on the BOD<sub>5</sub>/COD ratio is shown in Figs. 5(a) and (b). It can be seen that H<sub>2</sub>O<sub>2</sub> concentration has positive effects on the enhancement of biodegradability. It can be explained by the fact that more HO• generated at the high concentration of H<sub>2</sub>O<sub>2</sub> in the range of study [39]. However, when H<sub>2</sub>O<sub>2</sub> moves towards higher concentrations than 400 mM, a reduction in biodegradability can be seen. This reduction can be related to the scavenging of HO• radicals [3]. At high concentration of H<sub>2</sub>O<sub>2</sub>, perhydroxyl radicals generated instead of HO• radicals (Eq. (8)). These radicals are weaker oxidant than HO• radicals to decompose wastewater. Hence, the biodegradability decreased at high concentration of H<sub>2</sub>O<sub>2</sub>. Following equation shows the reaction of H<sub>2</sub>O<sub>2</sub> and HO• in aqueous solution [40,41]:



There is a maximum for BOD<sub>5</sub>/COD ratio when the pH varied from 3 to 9. It was observed that maximum BOD<sub>5</sub>/COD ratio was 0.877 which occurred at 400 mM concentration of H<sub>2</sub>O<sub>2</sub> and pH of 4.5.

### 3.5. Effect of pH and nano-Fe<sub>2</sub>O<sub>3</sub> concentration on BOD<sub>5</sub>/COD ratio

The contour and surface plots of BOD<sub>5</sub>/COD ratio vs. pH and nano-Fe<sub>2</sub>O<sub>3</sub> are shown in Figs. 6(a) and (b). It is clear that there is a maximum for BOD<sub>5</sub>/COD ratio when pH increased. In addition, nano-Fe<sub>2</sub>O<sub>3</sub> concentration has slightly positive effects on biodegradability of wastewater. Biodegradability

Table 3  
ANOVA results of response surface quadratic model for BOD<sub>5</sub>/COD ratio

Response 1	BOD/COD					
ANOVA for response surface quadratic model						
Analysis of variance table (partial sum of squares – Type III)						
Source	Sum of squares	df	Mean square	F value	p value, probability > F	
Model	1.48	14	0.11	74.89	<0.0001	Significant
A, pH	0.67	1	0.67	478.16	<0.0001	
B, time	0.041	1	0.041	29.20	<0.0001	
C, H <sub>2</sub> O <sub>2</sub>	0.039	1	0.039	27.86	<0.0001	
D, Fe <sup>3+</sup>	0.019	1	0.019	13.28	0.0024	
AB	0.014	1	0.014	10.23	0.0060	
AC	0.040	1	0.040	28.43	<0.0001	
AD	1.000E-004	1	1.000E-004	0.071	0.7934	
BC	7.225E-003	1	7.225E-003	5.13	0.0387	
BD	1.225E-003	1	1.225E-003	0.87	0.3656	
CD	2.250E-004	1	2.250E-004	0.16	0.6949	
A <sup>2</sup>	0.12	1	0.12	85.39	<0.0001	
B <sup>2</sup>	7.418E-005	1	7.418E-005	0.053	0.8215	
C <sup>2</sup>	7.938E-003	1	7.938E-003	5.64	0.0313	
D <sup>2</sup>	5.329E-003	1	5.329E-003	3.79	0.0706	
Residual	0.021	15	1.407E-003			
Lack of fit	0.016	10	1.562E-003	1.42	0.3653	Not significant
Pure error	5.483E-003	5	1.097E-003			
Corrected total	1.50	29				
Standard deviation	0.038		R-squared	0.9859		
Mean	0.62		Adjusted R-squared	0.9727		
CV, %	6.06		Predicted R-squared	0.9365		
PRESS	0.095		Adeq precision	25.700		

increased with increase in nano-Fe<sub>2</sub>O<sub>3</sub> concentration. For nano-Fe<sub>2</sub>O<sub>3</sub> concentration of more than 1.3 g L<sup>-1</sup>, biodegradability decreased by increasing concentration. The scavenging effect at a high concentration of nano-Fe<sub>2</sub>O<sub>3</sub> is the main reason for biodegradability reduction. In addition, accessible surface active sites of nanoparticles decreased at high nano-Fe<sub>2</sub>O<sub>3</sub> concentration because of the accumulation of nanoparticles at this condition [39].

In addition, another reason for decreasing BOD<sub>5</sub>/COD ratio at large amount of nano-Fe<sub>2</sub>O<sub>3</sub> is due to the negative effect of agglomeration on the penetration of UV light inside the solution. Due to this fact, decreasing of UV light penetration results in a reduction of the production rate of hydroxyl radicals. This leads to reduction of the biodegradation rate.

The maximum of BOD<sub>5</sub>/COD ratio is 0.86 that occurred at 1.3 g L<sup>-1</sup> concentration of nanoparticles when pH was 4.5.

### 3.6. Effect of time and H<sub>2</sub>O<sub>2</sub> concentration on BOD<sub>5</sub>/COD ratio

The effect of time and H<sub>2</sub>O<sub>2</sub> concentration on BOD<sub>5</sub>/COD ratio is shown in Figs. 7(a) and (b). It was observed that the biodegradability of wastewater increased with increasing H<sub>2</sub>O<sub>2</sub> concentration and time of reaction. The exposure of sample with the UV light will be lingered by increasing

the time of reaction and this result in increasing the rate of hydroxyl production. On the other hand, more amounts of hydroxyl radicals could be produced when H<sub>2</sub>O<sub>2</sub> and nano-Fe<sub>2</sub>O<sub>3</sub> have more reaction time. For H<sub>2</sub>O<sub>2</sub> concentration higher than 400 mM, a reduction in biodegradability is observed because of the scavenging effect.

The maximum biodegradability after 80 min of process reached to 0.87 when the H<sub>2</sub>O<sub>2</sub> concentration is 400 mM.

### 3.7. Effect of time and nano-Fe<sub>2</sub>O<sub>3</sub> concentration on BOD<sub>5</sub>/COD ratio

Figs. 8(a) and (b) show that the maximum biodegradability of wastewater is 0.86 for the concentration of 1.3 g L<sup>-1</sup> of nano-Fe<sub>2</sub>O<sub>3</sub> and reaction time of 80 min. The BOD<sub>5</sub>/COD ratio increased with increasing of both reaction time and nano-Fe<sub>2</sub>O<sub>3</sub> concentration less than 1.3 g L<sup>-1</sup>.

### 3.8. Effect of H<sub>2</sub>O<sub>2</sub> concentration and nano-Fe<sub>2</sub>O<sub>3</sub> concentration on BOD<sub>5</sub>/COD ratio

As shown in Figs. 9(a) and (b), BOD<sub>5</sub>/COD ratio increased by increasing H<sub>2</sub>O<sub>2</sub> concentration and nano-Fe<sub>2</sub>O<sub>3</sub> concentration. For a high concentration of H<sub>2</sub>O<sub>2</sub> (>400 mM) scavenging

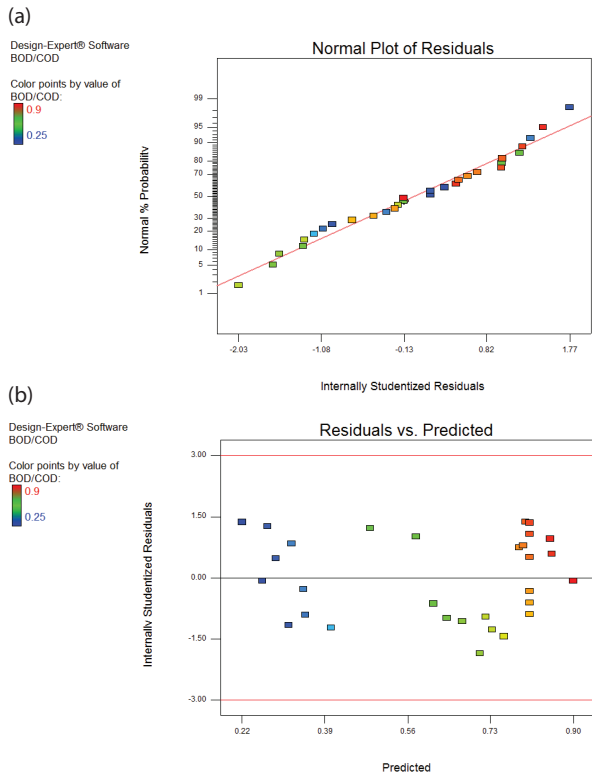


Fig. 3. (a) Normal probability plot of BOD<sub>5</sub>/COD ratio and (b) internally studentized residuals vs. predicted values of BOD<sub>5</sub>/COD ratio.

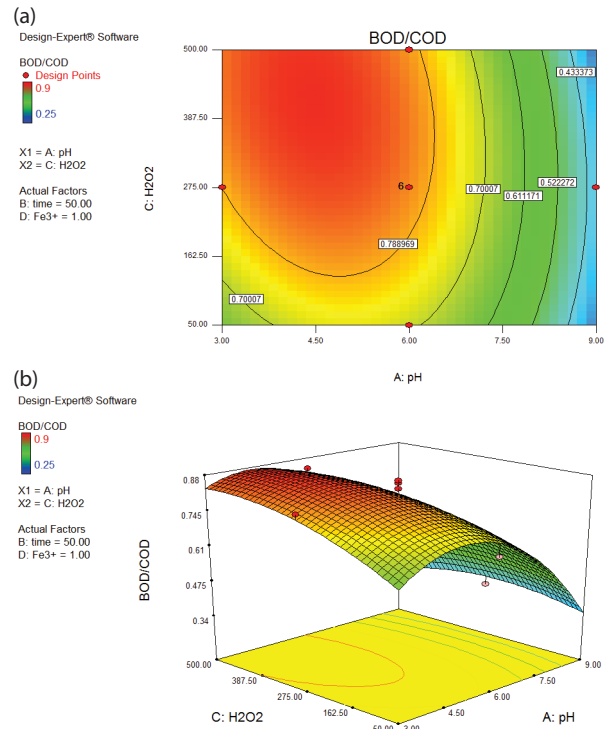


Fig. 5. Effect of pH and H<sub>2</sub>O<sub>2</sub> concentration on BOD<sub>5</sub>/COD ratio (a) contour plots and (b) 3D response surface.

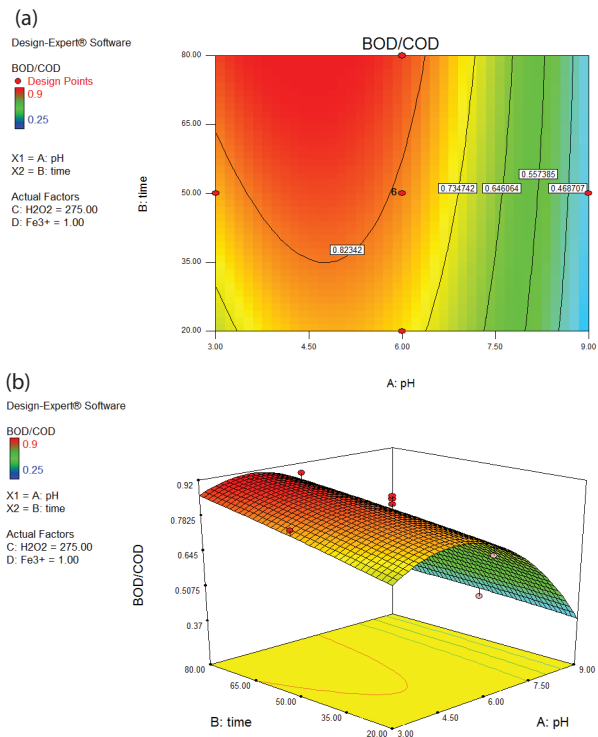


Fig. 4. Effect of pH and time on BOD<sub>5</sub>/COD ratio (a) contour plots (b) 3D response surface.

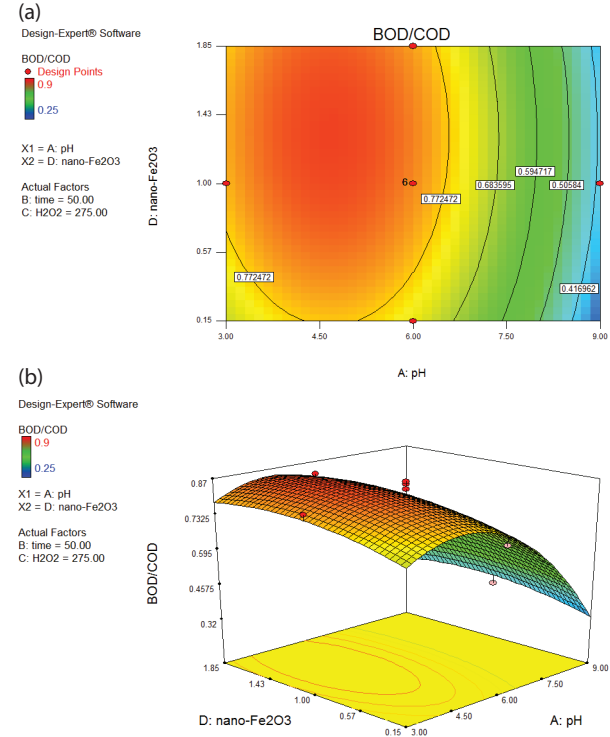


Fig. 6. Effect of pH and nano-Fe<sub>2</sub>O<sub>3</sub> concentration on BOD<sub>5</sub>/COD ratio (a) contour plots and (b) 3D response surface.

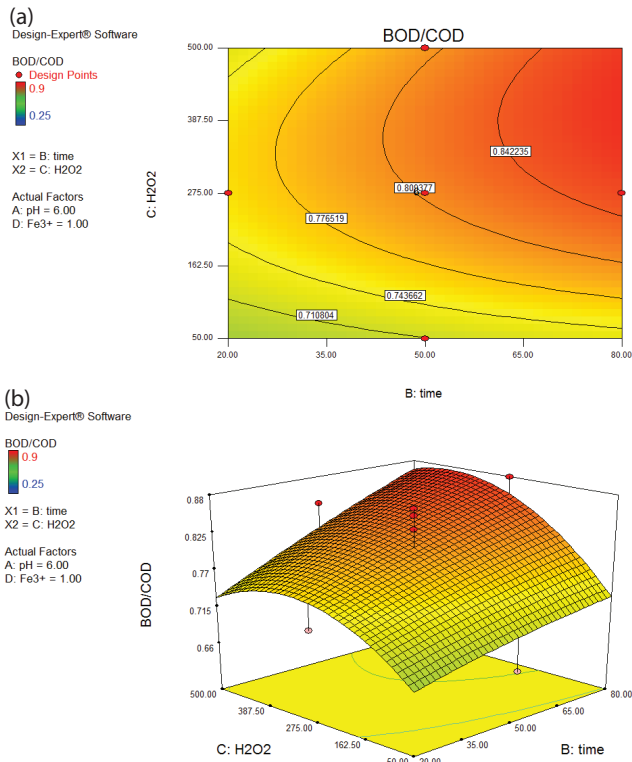


Fig. 7. Effect of reaction time and H<sub>2</sub>O<sub>2</sub> concentration on BOD<sub>5</sub>/COD ratio (a) contour plots and (b) 3D response surface.

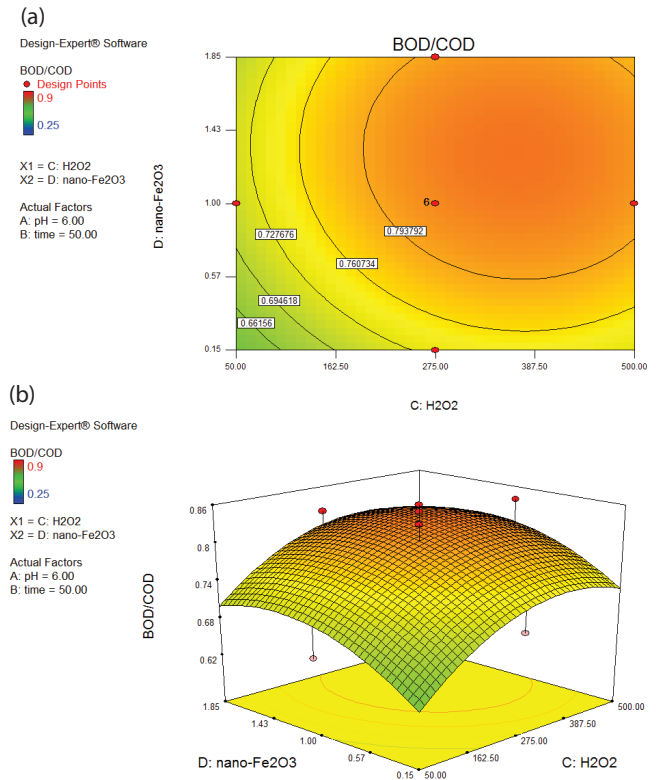


Fig. 9. Effect of H<sub>2</sub>O<sub>2</sub> and nano-Fe<sub>2</sub>O<sub>3</sub> concentration on BOD<sub>5</sub>/COD ratio (a) contour plots and (b) 3D response surface.

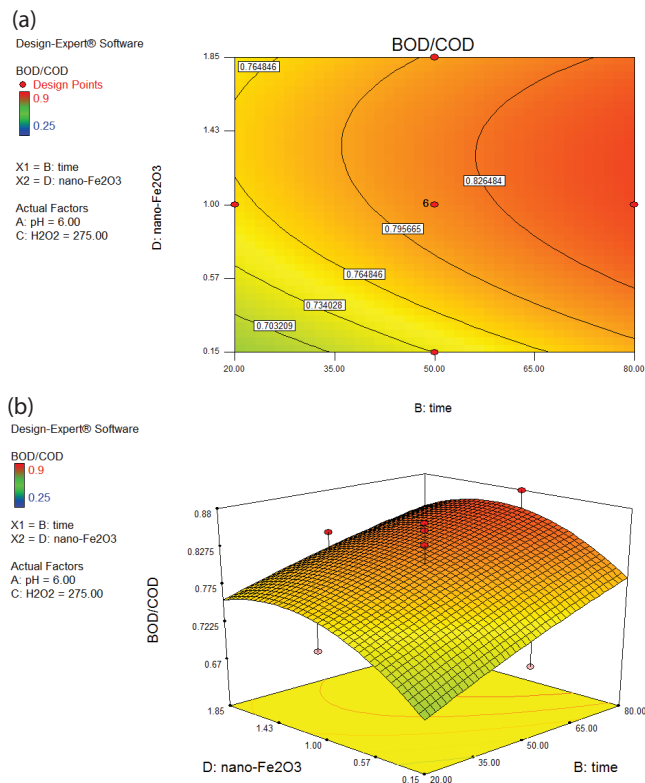


Fig. 8. Effect of reaction time and nano-Fe<sub>2</sub>O<sub>3</sub> concentration on BOD<sub>5</sub>/COD ratio (a) contour plots and (b) 3D response surface.

effect caused a reduction in biodegradability. Also for nano-Fe<sub>2</sub>O<sub>3</sub> concentration this reduction occurred at a concentration more than 1.3 g L<sup>-1</sup> due to scavenging effect and reduction of reachable active surface sites caused by agglomeration of nanoparticles.

Therefore, when H<sub>2</sub>O<sub>2</sub> concentrations are lower than 400 mM and nano-Fe<sub>2</sub>O<sub>3</sub> concentrations are lower than 1.3 g L<sup>-1</sup>, at a given concentration of H<sub>2</sub>O<sub>2</sub>, the production rate of hydroxyl radicals is mostly dependent on the nano-Fe<sub>3</sub>O<sub>4</sub> concentration and vice versa [39].

Therefore, maximum biodegradability of 0.82 occurred in 400 mM concentration of H<sub>2</sub>O<sub>2</sub> and 1.3 g L<sup>-1</sup> concentration of nano-Fe<sub>2</sub>O<sub>3</sub>.

### 3.9. Optimization

In order to obtain the optimum operating condition to have a biodegradable effluent (BOD<sub>5</sub>/COD = 0.5), Eq. (7) is considered as the objective function. The optimization was carried out by means of the numerical technique built in the Design Expert Software version 7. It searches the design space to achieve the goal of optimization in the range of independent factors. The optimum values to achieve the BOD<sub>5</sub>/COD = 0.50 at the range of neutral pH were pH = 7.49, reaction time = 21.66 min, H<sub>2</sub>O<sub>2</sub> concentration = 64 mM and nano-Fe<sub>2</sub>O<sub>3</sub> = 0.23 g L<sup>-1</sup>.

The obtained optimal operating conditions were used in another experimental run to validate the model prediction. Thus, 0.506 experimentally BOD<sub>5</sub>/COD ratio confirms the reliability of the model.

Table 4  
Kinetics experiment results

Time	(BOD <sub>5</sub> /COD) <sub>out</sub>
10	0.48
20	0.5
30	0.51
40	0.52
50	0.52
60	0.53
70	0.54
80	0.55

### 3.10. Kinetics experiment

In order to determine the removal mechanism kinetics, the process was repeated under the optimum condition for 80 min. Each sample was collected at 10 min intervals for analysis. The results are shown in Table 4.

In this study, the best appropriate model to explain kinetics of experiment was chosen according to the highest value of  $R^2$  among the most popular kinetic models. Zero-order, pseudo-first-order, and pseudo-second-order kinetic models were used in this research [10]:

$$[(BOD/COD)_t] = [(BOD/COD)_0] - Kt, \quad \text{zero-order} \quad (9)$$

$$\ln \left[ \frac{(BOD/COD)_t}{(BOD/COD)_0} \right] = Kt, \quad \text{pseudo-first-order} \quad (10)$$

$$\frac{1}{[(BOD/COD)_t]} = \frac{1}{[(BOD/COD)_0]} + Kt, \quad \text{pseudo-second-order} \quad (11)$$

where  $(BOD/COD)_0$  and  $(BOD/COD)_t$  are the value of BOD<sub>5</sub>/COD ratio of the solution at time 0 and at time  $t$ .  $K$  is the model constant in  $\text{min}^{-1}$  and  $t$  is the time in minutes [9].

Figs. 10(a)–(c) represent the model evaluation for BOD<sub>5</sub>/COD ratio. The correlation coefficient for the enhancement of BOD<sub>5</sub>/COD kinetics of zero-, pseudo-first- and second-order was obtained 0.9222, 0.9283 and 0.9308, respectively. So process follows the pseudo-second-order kinetic model.

### 4. Conclusion

The results demonstrated that the biodegradability of Direct Orange-26 wastewater can be successfully increased under a photo-Fenton-like process using a nano-Fe<sub>2</sub>O<sub>3</sub> catalyst.

An empirical relationship between BOD<sub>5</sub>/COD ratio and the studied factors (pH, reaction time, H<sub>2</sub>O<sub>2</sub> concentration and nano-Fe<sub>2</sub>O<sub>3</sub> concentration) were obtained.

The key parameter for the enhancement biodegradability of wastewater was pH. The effect of H<sub>2</sub>O<sub>2</sub> concentration is also important but to a smaller extent. The effect of reaction time and nano-Fe<sub>2</sub>O<sub>3</sub> concentration is less than that of others.

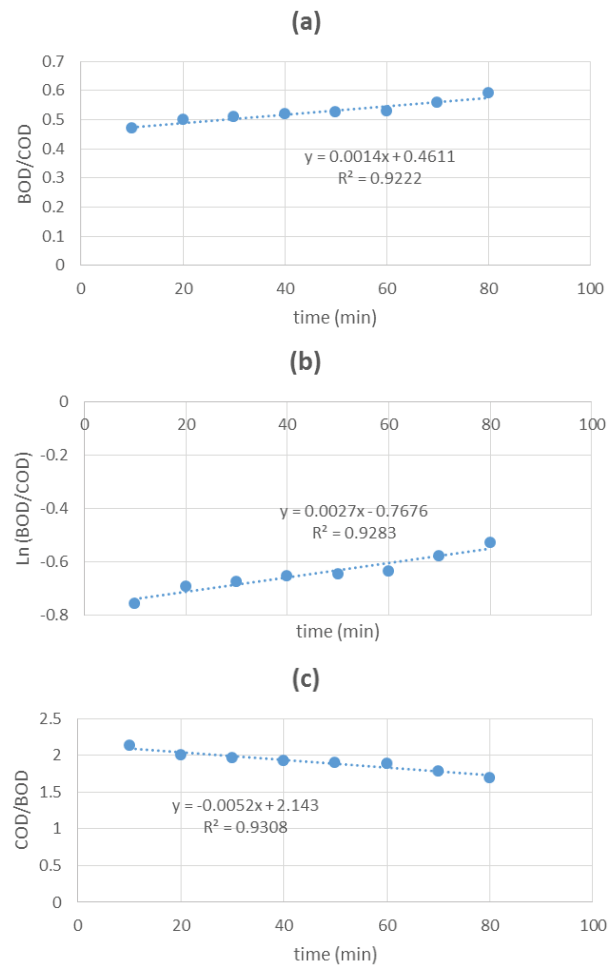


Fig. 10. (a) Zero-order, (b) pseudo-first-order and (c) pseudo-second-order kinetic modeling of enhancement biodegradability by photo-Fenton-like process.

### References

- [1] S.R. Pouran, A.R.A. Aziz, W.M.A.W. Daud, Review on the main advances in photo-Fenton oxidation system for recalcitrant wastewaters, *J. Ind. Eng. Chem.*, 21 (2015) 53–69.
- [2] R.K. Sheshdeh, M.R.K. Nikou, K. Badii, N.Y. Limae, G. Golkarnarenji, Equilibrium and kinetics studies for the adsorption of Basic Red 46 on nickel oxide nanoparticles-modified diatomite in aqueous solutions, *J. Taiwan Inst. Chem. Eng.*, 45 (2014) 1792–1802.
- [3] R.K. Sheshdeh, M.R.K. Nikou, K. Badii, S. Mohammadzadeh, Evaluation of adsorption kinetics and equilibrium for the removal of benzene by modified diatomite, *Chem. Eng. Technol.*, 36 (2013) 1713–1720.
- [4] S. Mohammadzadeh, M.E. Olya, A.M. Arabi, A. Shariati, M.R.K. Nikou, Synthesis, characterization and application of ZnO-Ag as a nanophotocatalyst for organic compounds degradation, mechanism and economic study, *J. Environ. Sci.*, 35 (2015) 194–207.
- [5] F. Asgharian, M.R.K. Nikou, B. Anvaripour, I. Danaee, Electrocoagulation and ultrasonic removal of humic acid from wastewater, *Environ. Prog. Sustainable Energy*, 36 (2016) 822–829.
- [6] R.K. Sheshdeh, S. Abbaszadeh, M.R.K. Nikou, K. Badii, M.S. Sharafi, Liquid phase adsorption kinetics and equilibrium of toluene by novel modified-diatomite, *J. Environ. Health Sci. Eng.*, 12 (2014) 148–157.

- [7] C.C. Amorim, M.M.D. Leão, R.F.P.M. Moreira, J.D. Fabris, A.B. Henriques, Performance of blast furnace waste for azo dye degradation through photo-Fenton-like processes, *Chem. Eng. J.*, 224 (2013) 59–66.
- [8] P. Bahmani, R.R. Kalantary, A. Esrafil, M. Gholami, A. J. Jafari, Evaluation of Fenton oxidation process coupled with biological treatment for the removal of reactive black 5 from aqueous solution, *J. Environ. Health Sci. Eng.*, 11 (2013) 1–9.
- [9] N.P. Tantak, S. Chaudhari, Degradation of azo dyes by sequential Fenton's oxidation and aerobic biological treatment, *J. Hazard. Mater.*, 136 (2006) 698–705.
- [10] Y. Safa, H.N. Bhatti, Kinetic and thermodynamic modeling for the removal of Direct Red-31 and Direct Orange-26 dyes from aqueous solutions by rice husk, *Desalination*, 272 (2011) 313–322.
- [11] I. Arslan-Alaton, G. Tureli, T. Olmez-Hanci, Treatment of azo dye production wastewaters using photo-Fenton-like advanced oxidation processes: optimization by response surface methodology, *J. Photochem. Photobiol., A*, 202 (2009) 142–153.
- [12] I. Oller, S. Malato, J.A. Sánchez-Pérez, Combination of advanced oxidation processes and biological treatments for wastewater decontamination—a review, *Sci. Total Environ.*, 409 (2011) 4141–4166.
- [13] K.M. Lee, S.B.A. Hamid, Simple response surface methodology: investigation on advance photocatalytic oxidation of 4-chlorophenoxyacetic acid using UV-active ZnO photocatalyst, *Materials*, 8 (2015) 339–354.
- [14] A.D. Bokare, W. Choi, Review of iron-free Fenton-like systems for activating  $H_2O_2$  in advanced oxidation processes, *J. Hazard. Mater.*, 275 (2014) 121–135.
- [15] A.L.N. Mota, L.F. Albuquerque, L.T.C. Beltrame, O. Chiavone-Filho, A. Machulek Jr., C.A.O. Nascimento, Advanced oxidation processes and their application in the petroleum industry: a review, *Braz. J. Pet. Gas*, 2 (2009) 122–142.
- [16] D. Hermosilla, M. Cortijo, C.P. Huang, Optimizing the treatment of landfill leachate by conventional Fenton and photo-Fenton processes, *Sci. Total Environ.*, 407 (2009) 3473–3481.
- [17] B. Ghasemi, B. Anvaripour, S. Jorfi, N. Jaafarzadeh, Enhanced photocatalytic degradation and mineralization of furfural using UVC/TiO<sub>2</sub>/GAC composite in aqueous solution, *Int. J. Photoenergy*, 2016 (2016) 1–10, Article ID. 2782607.
- [18] M. Swaminathan, M. Manickavachagam, M. Sillanpaa, Advanced oxidation processes for wastewater treatment, *Int. J. Photoenergy*, (2014) 1–3, Article ID. 682767.
- [19] S. Jorfi, G. Barzegar, M. Ahmadi, R.D.C. Soltani, A. Takdastan, R. Saeedi, M. Abtahi, Enhanced coagulation-photocatalytic treatment of Acid red 73 dye and real textile wastewater using UVA/synthesized MgO nanoparticles, *J. Environ. Manage.*, 177 (2016) 111–118.
- [20] A. Babuponnusami, K. Muthukumar, A review on Fenton and improvements to the Fenton process for wastewater treatment, *J. Environ. Chem. Eng.*, 2 (2014) 557–572.
- [21] C. Lee, J. Yoon, Temperature dependence of hydroxyl radical formation in the  $h\nu/Fe^{2+}/H_2O_2$  and  $Fe^{3+}/H_2O_2$  systems, *Chemosphere*, 56 (2004) 923–934.
- [22] R. Nogueira, A. Trovó, M. da Silva, R. Villa, Fundamentos e aplicações ambientais dos processos Fenton e foto-Fenton, *Química Nova*, 30 (2007) 400–408.
- [23] R. Zepp, B. Faust, J. Hoigne, Hydroxyl radical formation in aqueous reactions (pH 3–8) of iron(II) with hydrogen peroxide: the photo-Fenton reaction, *Environ. Sci. Technol.*, 26 (1992) 313–319.
- [24] J. Feng, X. Hu, P. L. Yue, H. Y. Zhu, G. Q. Lu, Degradation of azo-dye orange II by a photoassisted Fenton reaction using a novel composite of iron oxide and silicate nanoparticles as a catalyst, *Ind. Eng. Chem. Res.*, 42 (2003) 2058–2066.
- [25] K.E. Barrera-Salgado, G. Ramírez-Robledo, A. Álvarez-Gallegos, C.A. Pineda-Arellano, F.Z. Sierra-Espinosa, J.A. Hernández-Pérez, S. Silva-Martínez, Fenton process coupled to ultrasound and UV light irradiation for the oxidation of a model pollutant, *J. Chem.*, 2016 (2016) 1–7, Article ID. 4262530.
- [26] T. Matos, A. Dias, A. Reis, M. Silva, M.M. Kondo Degradation of abamectin using the photo-Fenton process, *Int. J. Chem. Eng.*, 2012 (2012) 1–7, Article ID. 915724.
- [27] B. Li, Y. Dong, Z. Ding, Y. Xu, C. Zou, Renovation and reuse of reactive dyeing effluent by a novel heterogeneous Fenton system based on metal modified PTFE fibrous catalyst/ $H_2O_2$ , *Int. J. Photoenergy*, 2013 (2013) 1–10, Article ID. 169493.
- [28] S. Ghafoori, M. Mehrvar, P.K. Chan, A statistical experimental design approach for photochemical degradation of aqueous polyacrylic acid using photo-Fenton-like process, *Polym. Degrad. Stab.*, 110 (2014) 492–497.
- [29] K. Rusevova, F.D. Kopinke, A. Georgi, Nano-sized magnetic iron oxides as catalysts for heterogeneous Fenton-like reactions— influence of Fe(II)/Fe(III) ratio on catalytic performance, *J. Hazard. Mater.*, 241 (2012) 433–440.
- [30] J. Shi, Z. Ai, L. Zhang, Fe@Fe<sub>2</sub>O<sub>3</sub> core-shell nanowires enhanced Fenton oxidation by accelerating the Fe(III)/Fe(II) cycles, *Water Res.*, 59 (2014) 145–153.
- [31] R. Soltani, S. Jorfi, M. Safari, M. Rajaei, Enhanced sonocatalysis of textile wastewater using bentonite-supported ZnO nanoparticles: response surface methodological approach, *J. Environ. Manage.*, 179 (2016) 47–57.
- [32] J. Sin, S. Lam, A. Mohamed, Optimizing photocatalytic degradation of phenol by TiO<sub>2</sub>/GAC using response surface methodology, *Korean J. Chem. Eng.*, 28 (2011) 84–92.
- [33] Y. Lin, C. Ferronato, N. Deng, F. Wu, J.M. Chovelon, Photocatalytic degradation of methylparaben by TiO<sub>2</sub>: multivariable experimental design and mechanism, *Appl. Catal., B*, 88 (2009) 32–41.
- [34] S.P. Sun, X. Zeng, A.T. Lemley, Kinetics and mechanism of carbamazepine degradation by a modified Fenton-like reaction with ferric-nitrilotriacetate complexes, *J. Hazard. Mater.*, 252 (2013) 155–165.
- [35] I. Arslan-Alaton, N. Ayten, T. Olmez-Hanci, Photo-Fenton-like treatment of the commercially important H-acid: process optimization by factorial design and effects of photocatalytic treatment on activated sludge inhibition, *Appl. Catal., B*, 96 (2010) 208–217.
- [36] M.A. Bezerra, R.E. Santelli, E.P. Oliveira, L.S. Villar, L.A. Escalera, Response surface methodology (RSM) as a tool for optimization in analytical chemistry, *Talanta*, 76 (2008) 965–977.
- [37] S. Ghafoori, M. Mehrvar, P. Chan, Optimisation of photo-Fenton-like degradation of aqueous polyacrylic acid using Box–Behnken experimental design, *Can. J. Chem. Eng.*, 92 (2014) 97–108.
- [38] S.P. Sun, X. Zeng, A.T. Lemley, Nano-magnetite catalyzed heterogeneous Fenton-like degradation of emerging contaminants carbamazepine and ibuprofen in aqueous suspensions and montmorillonite clay slurries at neutral pH, *J. Mol. Catal. A: Chem.*, 371 (2013) 94–103.
- [39] S.P. Sun, X. Zeng, C. Li, A.T. Lemley, Enhanced heterogeneous and homogeneous Fenton-like degradation of carbamazepine by nano-Fe<sub>3</sub>O<sub>4</sub>/H<sub>2</sub>O<sub>2</sub> with nitrilotriacetic acid, *Chem. Eng. J.*, 244 (2014) 44–49.
- [40] K. Chanderia, S. Kalal, J. Sharma, N. Ameta, P.B. Punjabi, Heterogeneous photo-Fenton like degradation of rhodamine B using copper loaded bentonite and H<sub>2</sub>O<sub>2</sub>, *Indian J. Chem.*, 52A (2013) 1416–1420.
- [41] S. Hwang, S.G. Huling, S. Ko, Fenton-like degradation of MTBE: effects of iron counter anion and radical scavengers, *Chemosphere*, 78 (2010) 563–568.